Generation and propagation of a partially coherent vector beam with special correlation functions

Yahong Chen,[1] Fei Wang,[1,*] Lin Liu,[1] Chengliang Zhao,[1] Yangjian Cai,[1,†] and Olga Korotkova[2]
[1]*School of Physical Science and Technology, Soochow University, Suzhou 215006, China*
[2]*Department of Physics, University of Miami, Coral Gables, Florida 33146, USA*
(Received 6 October 2013; published 2 January 2014)

We introduce a general optical system for synthesis of partially coherent vector beams with a variety of correlation functions. In particular we employ it for generation of the family of beams, termed the specially correlated radially polarized (SCRP) beams and examine their free-space propagation both theoretically and experimentally. Our results clearly show that a SCRP beam exhibits unique features on propagation in comparison with those of beams with conventional correlation functions. The technique for modulation of the correlation functions and, hence, the coherence state of a SCRP beam in the source plane leads to efficient control of its intensity distribution and its degree of polarization on propagation, which is of importance in particle trapping and material thermal processing applications.

DOI: 10.1103/PhysRevA.89.013801 PACS number(s): 42.25.Ja, 42.25.Kb, 41.85.Ew

I. INTRODUCTION

The states of coherence and polarization of light fields have been treated separately until very recently [1–3]. That is why it was commonly assumed that the state of polarization of a light beam is invariant as the beam propagates in free space: there was no inherent reason seen for its evolution. However, using a simple example, in 1994 James showed that the degree of polarization of a partially coherent light beam may in general change on propagation in free space [4]. In 1998, Gori [5], and in 2003, Wolf [6] introduced unified theories of coherence and polarization for partially coherent vector beams in time and frequency domains, respectively, showing that these properties are always intimately related [7]. Since then, numerous efforts have been made on characterization, generation, propagation, and detection of partially coherent vector beams due to their important applications in free-space optical communications, remote sensing, optical imaging, particle trapping, particle scattering, and material thermal processing [8–36].

Coherent vector beams can be classified as the ones with a spatially uniform state of polarization (e.g., linearly, circularly, and elliptically polarized beam) and with a spatially nonuniform state of polarization [e.g., radially polarized (RP), azimuthally polarized (AP), and cylindrical vector beams] [3,37–49]. In a similar way, partially coherent vector beams can also be classified as the ones with spatially uniform and spatially non-uniform state of polarization. The latter beams were introduced theoretically and generated experimentally only very recently [30–36], but have already found uses in free-space optical communication, particle trapping, and material thermal processing.

In all papers on the partially coherent vector beams cited above, the random beams have conventional correlation functions (i.e., Schell-model correlation functions). Only recently, partially coherent beams with nonconventional correlation functions have been introduced and examined [50–60]. They have been found to exhibit some extraordinary propagation characteristics, such as far-field flat-topped and ring intensity profile formation, self-focusing effect, and a lateral shift of the intensity maximum. With a few exceptions [61–63], the previous studies about partially coherent beams with nonconventional correlation functions were confined to scalar treatment. The superposition rules for constructing genuine spatial correlation functions of scalar and vector partially coherent beams were first discussed in Refs. [64] and [65], respectively. In this paper, our aim is to investigate the generation and propagation of a partially coherent vector beam with arbitrary correlation functions both theoretically and experimentally, and to analyze the obtained results.

II. PARTIALLY COHERENT VECTOR BEAM WITH SPECIAL CORRELATION FUNCTIONS

In this section, we briefly outline the sufficient condition for constructing the beam coherence-polarization (BCP) matrix in the space-time domain [or the cross-spectral density (CSD) matrix in the space-frequency domain] of a partially coherent vector beam, and then we introduce an optical system for generating a partially coherent vector beam with arbitrary correlation functions. Finally, we introduce the family of specially correlated radially polarized (SCRP) beams based on the proposed optical system.

Let us first consider a quasimonochromatic, partially coherent vector beam propagating, along the z direction. In the space-time domain, the second-order correlation properties of such a beam are characterized by the BCP matrix [5,66]

$$\hat{\Gamma}(\mathbf{r}_1,\mathbf{r}_2) = \begin{pmatrix} \Gamma_{xx}(\mathbf{r}_1,\mathbf{r}_2) & \Gamma_{xy}(\mathbf{r}_1,\mathbf{r}_2) \\ \Gamma_{yx}(\mathbf{r}_1,\mathbf{r}_2) & \Gamma_{yy}(\mathbf{r}_1,\mathbf{r}_2) \end{pmatrix}, \tag{1}$$

with elements

$$\Gamma_{\alpha\beta}(\mathbf{r}_1,\mathbf{r}_2) = \left\langle E_\alpha^*(\mathbf{r}_1) E_\beta(\mathbf{r}_2) \right\rangle, \quad (\alpha = x,y;\beta = x,y), \tag{2}$$

where $\mathbf{r}_1 \equiv (x_1,y_1)$ and $\mathbf{r}_2 \equiv (x_2,y_2)$ are two transverse position vectors, E_x and $E_y$denote the components of the random electric vector, along two mutually orthogonal x and y directions perpendicular to the z axis. The asterisk denotes the complex conjugate and the angular brackets denote ensemble average.

According to Ref. [65], in order for a BCP matrix to be genuine, i.e., physically realizable, it should satisfy the

*Corresponding author: fwang@suda.edu.cn
†Corresponding author: yangjiancai@suda.edu.cn

condition of non-negative definiteness, which is fulfilled if the elements of the BCP matrix have the following integral form:

$$\Gamma_{\alpha\beta}(\mathbf{r}_1,\mathbf{r}_2) = \int p_{\alpha\beta}(\mathbf{v}) H_\alpha^*(\mathbf{r}_1,\mathbf{v}) H_\beta(\mathbf{r}_2,\mathbf{v}) d^2\mathbf{v}, \times (\alpha = x,y;\beta = x,y), \quad (3)$$

where $\mathbf{v} \equiv (v_x, v_y)$, $H_x(\mathbf{r},\mathbf{v})$, and $H_y(\mathbf{r},\mathbf{v})$ are two arbitrary kernels, and $p_{\alpha\beta}(\mathbf{v})$ are the elements of the following weighting matrix

$$\hat{p}(\mathbf{v}) = \begin{pmatrix} p_{xx}(\mathbf{v}) & p_{xy}(\mathbf{v}) \\ p_{xy}^*(\mathbf{v}) & p_{yy}(\mathbf{v}) \end{pmatrix}. \quad (4)$$

The elements of the weighting matrix should satisfy the following conditions for any $\mathbf{v}$ [65]:

$$p_{xx}(\mathbf{v}) \geqslant 0, p_{yy}(\mathbf{v}) \geqslant 0, p_{xx}(\mathbf{v})\, p_{yy}(\mathbf{v}) - |p_{xy}(\mathbf{v})|^2 \geqslant 0. \quad (5)$$

One finds from Eqs. (3) and (5) that a variety of partially coherent vector beams with different BCP matrices can be introduced by choosing suitable $H_x(\mathbf{r},\mathbf{v})$, $H_y(\mathbf{r},\mathbf{v})$, and $\hat{p}(\mathbf{v})$.

Equation (3) can be rewritten in the following alternative form:

$$\Gamma_{\alpha\beta}(\mathbf{r}_1,\mathbf{r}_2) = \iint \Gamma_{\alpha\beta}(\mathbf{v}_1,\mathbf{v}_2) H_\alpha^*(\mathbf{r}_1,\mathbf{v}_1) H_\beta(\mathbf{r}_2,\mathbf{v}_2) \times d^2\mathbf{v}_1 d^2\mathbf{v}_2, (\alpha = x,y;\beta = x,y), \quad (6)$$

where

$$\Gamma_{\alpha\beta}(\mathbf{v}_1,\mathbf{v}_2) = E_\alpha^*(\mathbf{v}_1) E_\beta(\mathbf{v}_2) \delta(\mathbf{v}_1 - \mathbf{v}_2), \quad (7)$$

δ denoting the Dirac δ function. $\Gamma_{\alpha\beta}(\mathbf{v}_1,\mathbf{v}_2)$ and $\Gamma_{\alpha\beta}(\mathbf{r}_1,\mathbf{r}_2)$ can be regarded as the elements of the BCP matrix of the vector beam in the input plane and the output plane, respectively. The vector beam in the input plane is assumed to be incoherent. $H_x(\mathbf{r},\mathbf{v})$ and $H_y(\mathbf{r},\mathbf{v})$ are regarded as the response functions of the two paths through which $E_x(\mathbf{v})$ and $E_y(\mathbf{v})$ pass, respectively. Thus, one can generate a variety of partially coherent vector beams from an incoherent vector source through propagation by varying $E_x(\mathbf{v})$, $E_y(\mathbf{v})$, $H_x(\mathbf{r},\mathbf{v})$, and $H_y(\mathbf{r},\mathbf{v})$.

Figure 1 presents notations used for synthesis of a source generating a partially coherent vector beam with arbitrary correlation functions from an incoherent vector source. A thin lens L with focal length f and a Gaussian amplitude filter (GAF) with transmission function $T(\mathbf{r}) = \exp(-\mathbf{r}^2/4\sigma_0^2)$, σ_0^2

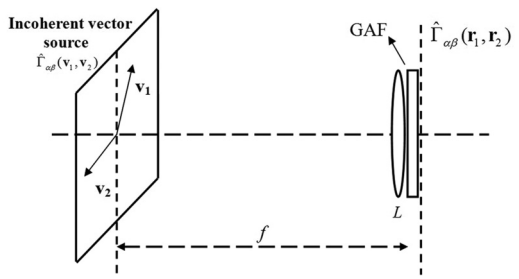

FIG. 1. Schematic diagram for generating a partially coherent vector beam with arbitrary correlation functions from an incoherent vector source. L, thin lens; GAF, Gaussian amplitude filter.

being the rms width, are located in the output plane. The distance between the source plane and the output plane is f. In our proposed optical system, the response functions $H_x(\mathbf{r},\mathbf{v})$ and $H_y(\mathbf{r},\mathbf{v})$ between the source plane and the output plane are the same and are expressed as

$$H_\alpha(\mathbf{r},\mathbf{v}) = \frac{-i}{\lambda f} T(\mathbf{r}) \exp\left[\frac{i\pi}{\lambda f}(\mathbf{v}^2 - 2\mathbf{r}\cdot\mathbf{v})\right], (\alpha = x,y). \quad (8)$$

After substituting Eqs. (7) and (8) into Eq. (6) we obtain

$$\Gamma_{\alpha\beta}(\mathbf{r}_1,\mathbf{r}_2) = \exp\left[-\frac{\mathbf{r}_1^2 + \mathbf{r}_2^2}{4\sigma_0^2}\right] \gamma_{\alpha\beta}\left[\frac{\mathbf{r}_2 - \mathbf{r}_1}{\lambda f}\right], \quad (9)$$

where

$$\gamma_{\alpha\beta}[(\mathbf{r}_2 - \mathbf{r}_1)/\lambda f] = \frac{1}{\lambda^2 f^2} \int \Gamma_{\alpha\beta}(\mathbf{v},\mathbf{v}) \times \exp\left[-\frac{i2\pi\mathbf{v}\cdot(\mathbf{r}_2 - \mathbf{r}_1)}{\lambda f}\right] d^2\mathbf{v}, \quad (10)$$

with $\Gamma_{\alpha\beta}(\mathbf{v},\mathbf{v}) = E_\alpha^*(\mathbf{v}) E_\beta(\mathbf{v})$. One finds from Eq. (10) that the correlation functions $\gamma_{\alpha\beta}$ of the elements of the BCP matrix of the generated partially coherent vector beam represent the Fourier transforms of the corresponding elements $\Gamma_{\alpha\beta}$ of the BCP matrix of the incoherent vector source with $\mathbf{v}_1 = \mathbf{v}_2 = \mathbf{v}$. If the elements of the BCP matrix of the incoherent vector source are Gaussian functions, i.e., $\Gamma_{\alpha\beta}(\mathbf{v},\mathbf{v}) = \exp[\mathbf{v}^2/\omega_{\alpha\beta}^2]$, we obtain the well-known electromagnetic Gaussian Schell-model beam (i.e., partially coherent vector beam with Gaussian Schell-model correlation functions) in the output plane [8,9]. By varying $E_x(\mathbf{v})$ and $E_y(\mathbf{v})$ of the incoherent vector source, one can generate a variety of partially coherent vector beams with different correlation functions in the output plane.

A partially coherent RP beam with conventional Schell-model correlation functions has been studied in detail both theoretically and experimentally [33–35]. As an application example, now we introduce the SCRP beam based on the proposed optical system. We assume that in Fig. 1 the source is an incoherent RP source, whose BCP matrix has the form [33–35]

$$\hat{\Gamma}(\mathbf{v}_1,\mathbf{v}_2) = \frac{1}{\omega_0^2} \exp\left(-\frac{\mathbf{v}_1^2 + \mathbf{v}_2^2}{\omega_0^2}\right) \times \begin{pmatrix} v_{1x}v_{2x} & v_{1x}v_{2y} \\ v_{1y}v_{2x} & v_{1y}v_{2y} \end{pmatrix} \delta(\mathbf{v}_1 - \mathbf{v}_2). \quad (11)$$

It can be easily verified that the elements of matrix $\hat{\Gamma}(\mathbf{v}_1,\mathbf{v}_2)$ satisfy the following constraints as required by Eq. (5):

$$\Gamma_{xx}(\mathbf{v},\mathbf{v}) \geqslant 0, \Gamma_{yy}(\mathbf{v},\mathbf{v}) \geqslant 0, \Gamma_{xx}(\mathbf{v},\mathbf{v})\,\Gamma_{yy}(\mathbf{v},\mathbf{v}) - |\Gamma_{xy}(\mathbf{v},\mathbf{v})|^2 \geqslant 0. \quad (12)$$

On substituting Eqs. (10) and (11) into Eq. (9), we obtain the following expressions for the elements of the BCP matrix of a SCRP beam:

$$\Gamma_{\alpha\alpha}(\mathbf{r}_1,\mathbf{r}_2) = C_0 \exp\left(-\frac{\mathbf{r}_1^2 + \mathbf{r}_2^2}{4\sigma_0^2}\right)\left(1 - \frac{(\alpha_2 - \alpha_1)^2}{\delta_0^2}\right) \times \exp\left[-\frac{(\mathbf{r}_1 - \mathbf{r}_2)^2}{2\delta_0^2}\right], (\alpha = x,y), \quad (13)$$

$$\Gamma_{xy}(\mathbf{r}_1,\mathbf{r}_2) = -C_0 \exp\left(-\frac{\mathbf{r}_1^2+\mathbf{r}_2^2}{4\sigma_0^2}\right)\frac{(x_2-x_1)(y_2-y_1)}{\delta_0^2} \times \exp\left[-\frac{(\mathbf{r}_1-\mathbf{r}_2)^2}{2\delta_0^2}\right], \quad (14)$$

$$\Gamma_{yx}(\mathbf{r}_1,\mathbf{r}_2) = \Gamma_{xy}^*(\mathbf{r}_2,\mathbf{r}_1), \quad (15)$$

where C_0 is a positive constant and $\delta_0 = \lambda f/\pi\omega_0$ represents the transverse coherence width of the RP beam with λ being the wavelength.

The intensity of the proposed partially coherent RP beam is given as [5,8,66]

$$I(\mathbf{r}) = \Gamma_{xx}(\mathbf{r},\mathbf{r}) + \Gamma_{yy}(\mathbf{r},\mathbf{r}) = 2C_0 \exp\left(-\frac{\mathbf{r}^2}{2\sigma_0^2}\right). \quad (16)$$

One finds that the intensity of the proposed SCRP beam in the source plane has a Gaussian beam profile.

In the literature there exist two definitions of the degree of coherence for a paraxial partially coherent vector beam [6–8,12]. For the convenience of comparison with later experimental results, we adopt here the definition introduced by Tervo *et al.* [12]. According to this definition, the degree of coherence $\gamma(\mathbf{r}_1,\mathbf{r}_2)$ of a partially coherent vector beam at a pair of transverse points with position vectors $\mathbf{r}_1$ and $\mathbf{r}_2$ has the form

$$\gamma^2(\mathbf{r}_1,\mathbf{r}_2) = \frac{\mathrm{Tr}[\hat{\Gamma}^\dagger(\mathbf{r}_1,\mathbf{r}_2)\hat{\Gamma}(\mathbf{r}_1,\mathbf{r}_2)]}{\mathrm{Tr}[\hat{\Gamma}(\mathbf{r}_1,\mathbf{r}_1)]\mathrm{Tr}[\hat{\Gamma}(\mathbf{r}_2,\mathbf{r}_2)]}. \quad (17)$$

where Tr represents the trace of matrix, the symbol † denotes the Hermitian adjoint.

Applying Eqs. (13)–(15) and (17), we calculate in Fig. 2 the density plots of the square of the degree of coherence γ^2, the square of the correlation functions γ_{xx}^2, γ_{yy}^2, and γ_{xy}^2 of the SCRP beam in the source plane. The correlation parameter used in the calculations is set as $\delta_0 = 0.5$ mm. One finds from Fig. 2 that the distributions of γ^2, γ_{xx}^2, γ_{yy}^2, and γ_{xy}^2 of the proposed SCRP beam in the source plane all have non-Gaussian profiles, in striking contrast with those of the partially coherent RP beam with the conventional Schell-model correlation functions in the source plane whose distributions of γ^2, γ_{xx}^2, γ_{yy}^2, and γ_{xy}^2 all have Gaussian profiles. In the next sections, we will show both theoretically and experimentally that on propagation in free space the special correlation functions lead to unique evolution features in all the second-order properties of a partially coherent RP beam.

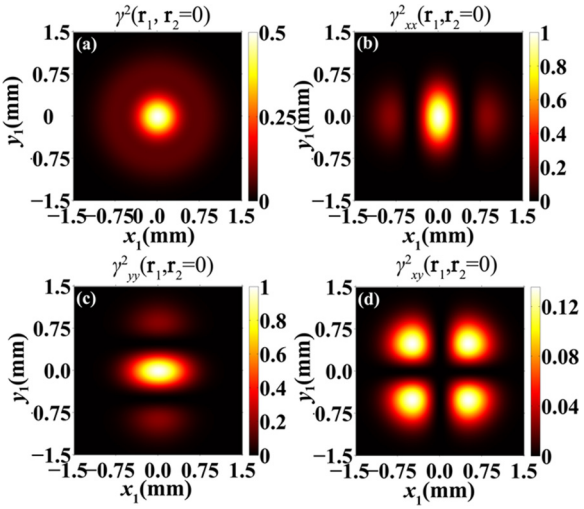

FIG. 2. (Color online) Density plots of (a) the square of the degree of coherence $\gamma^2(\mathbf{r}_1,\mathbf{r}_2=0)$, (b)–(d) the square of the correlation functions $\gamma_{xx}^2(\mathbf{r}_1,\mathbf{r}_2=0)$, $\gamma_{yy}^2(\mathbf{r}_1,\mathbf{r}_2=0)$, and $\gamma_{xy}^2(\mathbf{r}_1,\mathbf{r}_2=0)$, of the SCRP beam in the source plane.

III. PROPAGATION OF A SCRP BEAM

In this section, we derive the analytical propagation law for the SCRP beam proposed in the previous section, and examine its outcomes.

Within the validity of the paraxial approximation, the propagation of the elements of the BCP matrix of a partially coherent vector beam through a stigmatic ABCD optical system can be studied with the help of the following extended Collins formula [67,68]

$$\begin{aligned}\Gamma_{\alpha\beta}(\boldsymbol{\rho}_1,\boldsymbol{\rho}_2) = \left(\frac{1}{\lambda|B|}\right)^2 &\int_{-\infty}^{\infty}\int_{-\infty}^{\infty}\int_{-\infty}^{\infty}\int_{-\infty}^{\infty} \times \Gamma_{\alpha\beta}(\mathbf{r}_1,\mathbf{r}_2)dx_1dx_2dy_1dy_2 \\ &\times \exp\left[-\frac{ik}{2B}\left(Ax_1^2 - 2x_1\rho_{1x} + D\rho_{1x}^2\right)\right. \\ &\left. -\frac{ik}{2B}\left(Ay_1^2 - 2y_1\rho_{1y} + D\rho_{1y}^2\right)\right] \\ &\times \exp\left[\frac{ik}{2B}\left(Ax_2^2 - 2x_2\rho_{2x} + D\rho_{2x}^2\right)\right. \\ &\left. +\frac{ik}{2B}\left(Ay_2^2 - 2y_2\rho_{2y} + D\rho_{2y}^2\right)\right], \end{aligned} \quad (18)$$

where $\boldsymbol{\rho}_1 \equiv (\rho_{1x},\rho_{1y})$ and $\boldsymbol{\rho}_2 \equiv (\rho_{2x},\rho_{2y})$ are two arbitrary transverse position vectors in the field, A, B, C, and D are the elements of the transfer matrix of the optical system.

Substituting Eqs. (13)–(15) into Eq. (18), we obtain the following analytical expressions for the elements of the BCP matrix of the propagating SCRP beam

$$\Gamma_{\alpha\alpha}(\boldsymbol{\rho}_1,\boldsymbol{\rho}_2) = C_0\frac{\sigma_0^2}{S_0^2}\left[1 + \frac{B^2}{k^2\delta_0^2S_0^2}\left(\frac{T_{\alpha\alpha}\sigma_0^4}{S_0^2} - 1\right)\right]S(\boldsymbol{\rho}_1,\boldsymbol{\rho}_2), \quad (19)$$

$$\Gamma_{xy}(\boldsymbol{\rho}_1,\boldsymbol{\rho}_2) = C_0\frac{\sigma_0^2}{S_0^2}\frac{T_{xy}\sigma_0^4B^2}{\delta_0^2k^2S_0^4}S(\boldsymbol{\rho}_1,\boldsymbol{\rho}_2), \quad (20)$$

$$\Gamma_{yx}(\boldsymbol{\rho}_1,\boldsymbol{\rho}_2) = \Gamma_{xy}^*(\boldsymbol{\rho}_2,\boldsymbol{\rho}_1), \quad (21)$$

with

$$S(\boldsymbol{\rho}_1,\boldsymbol{\rho}_2) = \exp\left[\frac{ik}{2B}\left(D - \frac{A\sigma_0^2}{S_0^2}\right)\left(\boldsymbol{\rho}_2^2 - \boldsymbol{\rho}_1^2\right) - \frac{(\boldsymbol{\rho}_1+\boldsymbol{\rho}_2)^2}{8S_0^2} - \frac{(\boldsymbol{\rho}_1-\boldsymbol{\rho}_2)^2}{8S_0^2}\left(1 + \frac{4\sigma_0^2}{\delta_0^2}\right)\right], \quad (22)$$

$$S_0^2 = \sigma_0^2\left[A^2 + \left(1 + \frac{4\sigma_0^2}{\delta_0^2}\right)\left(\frac{B}{2k\sigma_0^2}\right)^2\right], \tag{23}$$

$$T_{\alpha\alpha} = \left[\frac{\rho_{1\alpha} + \rho_{2\alpha}}{2\sigma_0^2} + \frac{ikA\,(\rho_{2\alpha} - \rho_{1\alpha})}{B}\right]^2, (\alpha = x, y), \tag{24}$$

$$T_{xy} = \left[\frac{\rho_{1x} + \rho_{2x}}{2\sigma_0^2} + \frac{ikA\,(\rho_{2x} - \rho_{1x})}{B}\right] \times \left[\frac{\rho_{1y} + \rho_{2y}}{2\sigma_0^2} + \frac{ikA(\rho_{2y} - \rho_{1y})}{B}\right]. \tag{25}$$

The intensity of the propagating SCRP beam is given as

$$I(\boldsymbol{\rho}) = \Gamma_{xx}(\boldsymbol{\rho}, \boldsymbol{\rho}) + \Gamma_{yy}(\boldsymbol{\rho}, \boldsymbol{\rho}). \tag{26}$$

Applying Eqs. (19)–(26), one can numerically study the propagation of the SCRP in a convenient way. As a particular example, we will now consider the focusing properties of the SCRP beam. Assume that the beam passes through a thin lens with focal length f and then arrives at the plane$\boldsymbol{\rho}$. The distances from the source to the thin lens and from the thin lens to the plane$\boldsymbol{\rho}$are f and z, respectively. The transfer matrix between the source plane and the plane $\boldsymbol{\rho}$ reads as

$$\begin{pmatrix} A & B \\ C & D \end{pmatrix} = \begin{pmatrix} 1 & z \\ 0 & 1 \end{pmatrix}\begin{pmatrix} 1 & 0 \\ -1/f & 1 \end{pmatrix}\begin{pmatrix} 1 & f \\ 0 & 1 \end{pmatrix} = \begin{pmatrix} 1 - z/f & f \\ -1/f & 0 \end{pmatrix}. \tag{27}$$

We show in Fig. 3 the density plot of the normalized intensity distribution and the corresponding cross line of the focused SCRP beam with $f = 400\,\text{mm}$, $\lambda = 632.8\,\text{nm}$, $\sigma_0 = 1\,\text{mm}$, and $\delta_0 = 0.25\,\text{mm}$ at several propagation distances. One finds

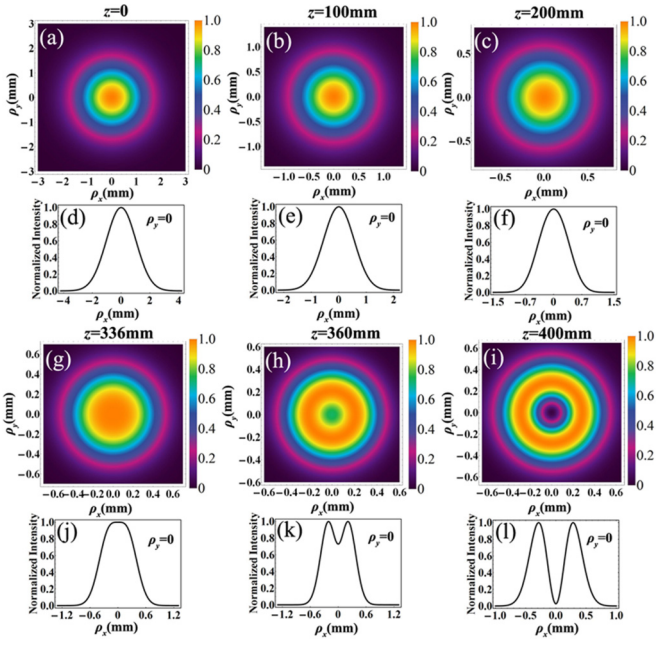

FIG. 3. (Color online) Density plot of the normalized intensity distribution and the corresponding cross line of the focused SCPR beam at several propagation distances.

from Fig. 3 that on propagation the beam of interest exhibits unique properties, which are quite different from those of the RP beam with Schell-model correlation functions [33]. For the SCRP beam, the intensity distribution of such a beam in the source plane ($z = 0$) is Gaussian, while its intensity distribution in the geometrical focal plane ($z = 400$ mm) evolves into a dark hollow profile when its initial coherence width is small ($\delta_0 = 0.25$ mm). Further, a flat-topped beam intensity profile can be formed at suitable propagation distance ($z = 336$ mm). In comparison, the intensity distribution of the RP beam with Schell-model correlation functions has a dark hollow profile in the source plane, evolving into a Gaussian profile in the geometrical focal plane when its initial coherence width is small [33].

To learn about the influence of the initial coherence width δ_0 on the focused intensity distribution, we calculate in Fig. 4 the density plot of the normalized intensity distribution and the corresponding cross line of the SCRP beam in the geometrical focal plane ($z = f$) for different values of the initial coherence width δ_0 with $f = 400\,\text{mm}$, $\lambda = 632.8\,\text{nm}$, and $\sigma_0 = 1\,\text{mm}$. One finds that the dependence of the focused intensity distribution of the SCRP beam on the initial coherence width is also very different from that of the RP beam with conventional Schell-model correlation functions. For the SCRP beam, the intensity distribution in the geometrical focal plane gradually changes from a dark hollow profile to a Gaussian beam profile as the value of the initial coherence width increases, and a flat-topped beam profile can be formed for a suitable value of the initial coherence width. In contrast, for the RP beam with Schell-model correlation functions, the intensity distribution in the geometrical focal plane gradually changes from a Gaussian beam profile to a dark hollow beam profile as the value of the initial coherence width increases [33]. Thus, modulating the correlation function of the RP beam provides a convenient way for shaping its focused beam profile, which will be useful in particle trapping, where a focused Gaussian beam or flat-topped beam profile is required for trapping a particle with refractive index larger than that of the ambient and a focused dark hollow beam profile is required for trapping a particle with refractive index smaller than that of the ambient [3,32,69,70]. It is also of use in material thermal processing and inertial confinement fusion where a focused flat-topped beam profile is required [71,72].

Now we study the polarization properties of the SCRP beam on propagation after passing the thin lens. The BCP matrix of a partially coherent vector beam at point $\boldsymbol{\rho}$ can be locally represented as a sum of a completely unpolarized beam and a completely polarized beam [8,10]

$$\hat{\Gamma}(\boldsymbol{\rho}, \boldsymbol{\rho}) = \hat{\Gamma}^{(u)}(\boldsymbol{\rho}, \boldsymbol{\rho}) + \hat{\Gamma}^{(p)}(\boldsymbol{\rho}, \boldsymbol{\rho}), \tag{28}$$

where

$$\hat{\Gamma}^{(u)}(\boldsymbol{\rho}, \boldsymbol{\rho}) = \begin{pmatrix} A(\boldsymbol{\rho}, \boldsymbol{\rho}) & 0 \\ 0 & A(\boldsymbol{\rho}, \boldsymbol{\rho}) \end{pmatrix}, \tag{29}$$

$$\hat{\Gamma}^{(p)}(\boldsymbol{\rho}, \boldsymbol{\rho}) = \begin{pmatrix} B(\boldsymbol{\rho}, \boldsymbol{\rho}) & D(\boldsymbol{\rho}, \boldsymbol{\rho}) \\ D^*(\boldsymbol{\rho}, \boldsymbol{\rho}) & C(\boldsymbol{\rho}, \boldsymbol{\rho}) \end{pmatrix}, \tag{30}$$

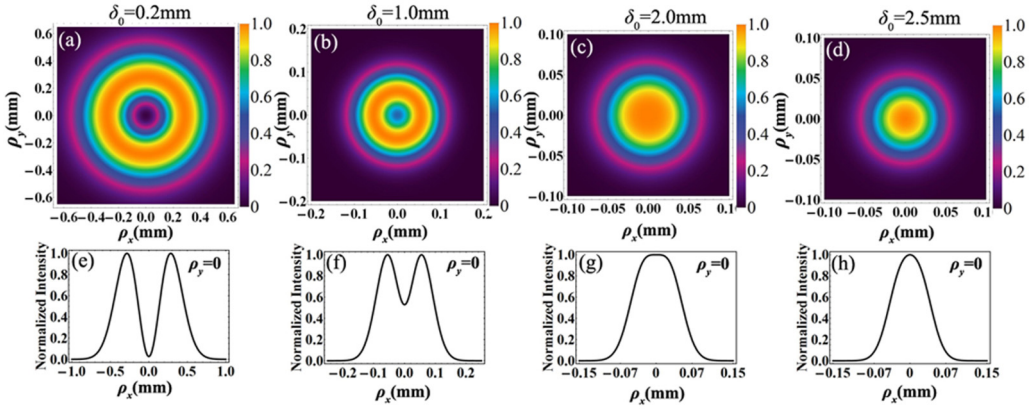

FIG. 4. (Color online) Density plots of the normalized intensity distribution and the corresponding cross line of the SCRP beam in the geometrical focal plane ($z = f$) for different values of the initial coherence widthδ_0.

with

$$A(\boldsymbol{\rho},\boldsymbol{\rho}) = \frac{1}{2}[\Gamma_{xx}(\boldsymbol{\rho},\boldsymbol{\rho}) + \Gamma_{yy}(\boldsymbol{\rho},\boldsymbol{\rho}) - \sqrt{[\Gamma_{xx}(\boldsymbol{\rho},\boldsymbol{\rho}) - \Gamma_{yy}(\boldsymbol{\rho},\boldsymbol{\rho})]^2 + 4|\Gamma_{xy}(\boldsymbol{\rho},\boldsymbol{\rho})|^2}], \tag{31}$$

$$B(\boldsymbol{\rho},\boldsymbol{\rho}) = \frac{1}{2}[\Gamma_{xx}(\boldsymbol{\rho},\boldsymbol{\rho}) - \Gamma_{yy}(\boldsymbol{\rho},\boldsymbol{\rho}) + \sqrt{[\Gamma_{xx}(\boldsymbol{\rho},\boldsymbol{\rho}) - \Gamma_{yy}(\boldsymbol{\rho},\boldsymbol{\rho})]^2 + 4|\Gamma_{xy}(\boldsymbol{\rho},\boldsymbol{\rho})|^2}], \tag{32}$$

$$C(\boldsymbol{\rho},\boldsymbol{\rho}) = \frac{1}{2}[\Gamma_{yy}(\boldsymbol{\rho},\boldsymbol{\rho}) - \Gamma_{xx}(\boldsymbol{\rho},\boldsymbol{\rho}) + \sqrt{[\Gamma_{xx}(\boldsymbol{\rho},\boldsymbol{\rho}) - \Gamma_{yy}(\boldsymbol{\rho},\boldsymbol{\rho})]^2 + 4|\Gamma_{xy}(\boldsymbol{\rho},\boldsymbol{\rho})|^2}], \tag{33}$$

$$D(\boldsymbol{\rho},\boldsymbol{\rho}) = \Gamma_{xy}(\boldsymbol{\rho},\boldsymbol{\rho}). \tag{34}$$

Applying Eqs. (19)–(25), we obtain the following expressions for $\hat{\Gamma}^{(u)}(\boldsymbol{\rho},\boldsymbol{\rho})$ and $\hat{\Gamma}^{(p)}(\boldsymbol{\rho},\boldsymbol{\rho})$

$$\hat{\Gamma}^{(u)}(\boldsymbol{\rho},\boldsymbol{\rho}) = C_0\frac{\sigma_0^4}{S_0^4}\left(A^2 + \left(\frac{B}{2k\sigma_0^2}\right)^2\right)\exp\left[-\frac{\boldsymbol{\rho}^2}{2S_0^2}\right] \times \begin{pmatrix} 1 & 0 \\ 0 & 1 \end{pmatrix}, \tag{35}$$

$$\hat{\Gamma}^{(p)}(\boldsymbol{\rho},\boldsymbol{\rho}) = C_0\frac{\sigma_0^2}{\delta_0^2 S_0^6}\left(\frac{B}{k}\right)^2\exp\left[-\frac{\boldsymbol{\rho}^2}{2S_0^2}\right] \times \begin{pmatrix} \rho_x^2 & \rho_x\rho_y \\ \rho_x\rho_y & \rho_y^2 \end{pmatrix}. \tag{36}$$

The state of polarization of the completely polarized beam can be characterized by the polarization ellipse. The major and minor semiaxes of the polarization ellipse, A_1 and A_2, as well as its degree of ellipticity, ε, and its orientation angle, θ, are related to the elements of the BCP matrix $\hat{\Gamma}$ by the following formulas

$$A_{1,2}(\boldsymbol{\rho}) = \frac{1}{\sqrt{2}}\Big[\sqrt{\left[\Gamma_{xx}^{(p)}(\boldsymbol{\rho},\boldsymbol{\rho}) - \Gamma_{yy}^{(p)}(\boldsymbol{\rho},\boldsymbol{\rho})\right]^2 + 4\left|\Gamma_{xy}^{(p)}(\boldsymbol{\rho},\boldsymbol{\rho})\right|^2} \pm \sqrt{\left[\Gamma_{xx}^{(p)}(\boldsymbol{\rho},\boldsymbol{\rho}) - \Gamma_{yy}^{(p)}(\boldsymbol{\rho},\boldsymbol{\rho})\right]^2 + 4\mathrm{Re}\left[\Gamma_{xy}^{(p)}(\boldsymbol{\rho},\boldsymbol{\rho})\right]^2}\Big]^{1/2}, \tag{37}$$

$$\varepsilon(\boldsymbol{\rho},z) = A_2(\boldsymbol{\rho})/A_1(\boldsymbol{\rho}), \tag{38}$$

$$\theta(\rho) = \frac{1}{2}\arctan\left[\frac{2\mathrm{Re}\left[\Gamma_{xy}^{(p)}(\boldsymbol{\rho},\boldsymbol{\rho})\right]}{\Gamma_{xx}^{(p)}(\boldsymbol{\rho},\boldsymbol{\rho}) - \Gamma_{yy}^{(p)}(\boldsymbol{\rho},\boldsymbol{\rho})}\right]. \tag{39}$$

In Eq. (37), signs "+" and "−" between the two square roots correspond to A_1 and A_2, respectively. "Re" stands for taking the real part. Substituting Eq. (36) into Eqs. (37)–(39), we obtain

$$A_2(\boldsymbol{\rho}) = 0, \varepsilon(\boldsymbol{\rho}) = 0, \theta(\boldsymbol{\rho}) = \arctan[\rho_y/\rho_x]. \tag{40}$$

One finds from Eq. (40) that the completely polarized part of the partially coherent RP beam has a radial polarization and the state of polarization remains invariant on propagation.

The intensity distributions of the completely polarized and completely unpolarized parts of the partially coherent RP beam are given, respectively, as

$$I^{(p)}(\boldsymbol{\rho}) = \Gamma_{xx}^{(p)}(\boldsymbol{\rho},\boldsymbol{\rho}) + \Gamma_{yy}^{(p)}(\boldsymbol{\rho},\boldsymbol{\rho}), \tag{41}$$

and

$$I^{(u)}(\boldsymbol{\rho}) = \Gamma_{xx}^{(u)}(\boldsymbol{\rho},\boldsymbol{\rho}) + \Gamma_{yy}^{(u)}(\boldsymbol{\rho},\boldsymbol{\rho}). \tag{42}$$

In Fig. 5 we calculate the cross lines of the normalized intensity distributions$I^{(p)}(\rho_x,0)/I(\mathbf{r}=0)$,$I^{(u)}(\rho_x,0)/I(\mathbf{r}=0)$, $I(\rho_x,0)/I(\mathbf{r}=0)$ of the focused SCRP beam at several propagation distances for different values of the initial coherence width δ_0 with $f = 400\,\mathrm{mm}$, $\lambda = 632.8\,\mathrm{nm}$, and $\sigma_0 = 1\mathrm{mm}$. Here $I(\mathbf{r}=0)$ represents the intensity distribution of the beam at point $\mathbf{r} = 0$ in the source plane. The intensity distribution of the completely polarized part has a dark hollow beam profile, and the intensity distribution of the completely unpolarized

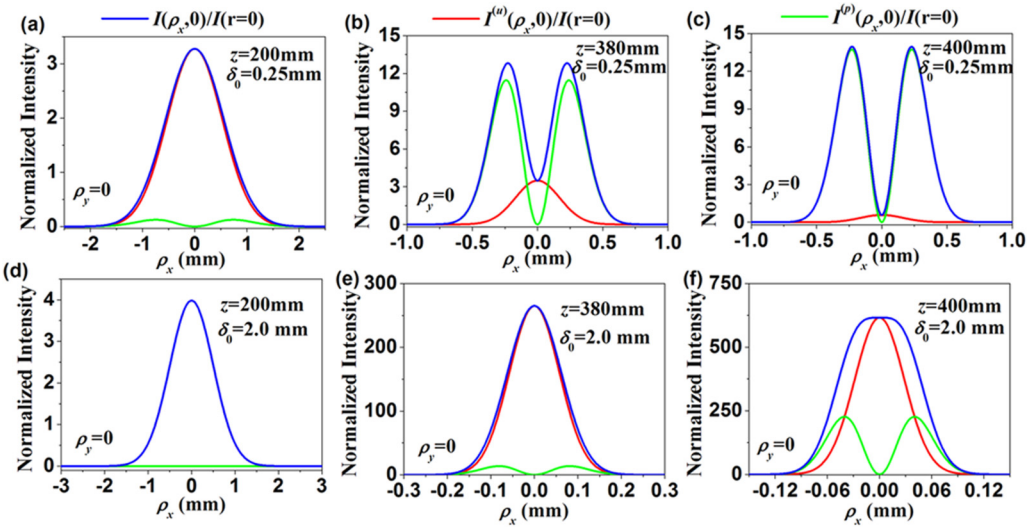

FIG. 5. (Color online) Cross lines of the normalized intensity distributions $I^{(p)}(\rho_x,0)/I\,(\mathbf{r}=0)$,$I^{(u)}(\rho_x,0)/I\,(\mathbf{r}=0)$,$I(\rho_x,0)/I\,(\mathbf{r}=0)$ of the focused SCRP beam at several propagation distances for different values of the initial coherence width δ_0.

part has a Gaussian beam profile. The total intensity distribution is determined by the intensity distributions of two parts together. When the propagation distance is short (z = 200 mm), the contribution of the completely unpolarized part plays a dominant role, thus the total intensity distribution has a Gaussian beam profile [see Figs. 5(a) and 5(d)]. With the increase of the propagation distance, the contribution of the completely polarized part gradually increases. For the case of $\delta_0 = 0.25$ mm, the contribution of the completely polarized part plays a dominant role in the geometrical focal plane, thus the total intensity distribution has a dark hollow beam profile [see Fig. 5(c)]. For the case of $\delta_0 = 2$ mm, the contribution of the completely unpolarized part is the same as that of the completely polarized part in the geometrical focal plane (see Fig. 6), thus the total intensity distribution exhibits a flat-topped beam profile [see Fig. 5(f)].

To learn about the power transition from the completely unpolarized part to the completely polarized part on propagation in detail, now we study the evolution of the normalized power of the completely unpolarized part or polarized part, which is defined as

$$\eta^{(l)}(z) = \frac{\int I^{(l)}(\boldsymbol{\rho})d^2\boldsymbol{\rho}}{\int I(\boldsymbol{\rho})d^2\boldsymbol{\rho}}, (l = u, p), \tag{43}$$

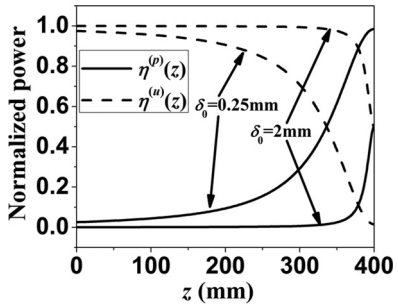

FIG. 6. Variation of the normalized powers of the completely unpolarized part and the completely polarized part of the focused SCRP beam with special correlation functions versus the propagation distance for different values of the initial coherence width δ_0.

where $\eta^{(u)}(z)$ and $\eta^{(p)}(z)$ represent the normalized powers of the completely unpolarized part and the completely polarized part, respectively. We calculate in Fig. 6 the variation of the normalized powers of the completely unpolarized part and the completely polarized part of the focused SCRP beam versus the propagation distance for different values of the initial coherence width δ_0 with $f = 400$ mm, $\lambda = 632.8$ nm, and $\sigma_0 = 1$mm. The normalized power $\eta^{(u)}(z)$ of the completely unpolarized part decreases on propagation, while the normalized power $\eta^{(p)}(z)$ of the completely polarized part increases. The power transition from the completely unpolarized part to the completely polarized part occurs rapidly with the decrease of the initial coherence width δ_0. For the case of $\delta_0 = 0.25$ mm, $\eta^{(p)}(z)$ reaches to 98.5%, which means the SCRP beam in the geometrical focal plane becomes almost completely polarized. For the case of $\delta_0 = 2$ mm, both $\eta^{(p)}(z)$ and $\eta^{(u)}(z)$ attain the value of 0.5, implying that the contributions of the completely polarized part and the completely unpolarized part are the same. The results shown in Figs. 5 and 6 are strikingly different from those of the RP beam with Schell-model correlation functions [34]: for such a beam the power of the completely polarized part transits to the completely unpolarized part on propagation, and the beam becomes almost completely unpolarized in the geometrical focal plane when the initial coherence width δ_0 is small.

The degree of polarization of a partially coherent vector beam is defined as [8]

$$P(\boldsymbol{\rho}) = \frac{I^{(p)}(\boldsymbol{\rho})}{I(\boldsymbol{\rho})} = \sqrt{1 - \frac{4\mathrm{Det}[\hat{\Gamma}(\boldsymbol{\rho},\boldsymbol{\rho})]}{[\mathrm{Tr}\hat{\Gamma}(\boldsymbol{\rho},\boldsymbol{\rho})]^2}}. \tag{44}$$

Applying Eqs. (19)–(25) and (43) we obtain for the degree of polarization a SCRP beam, the following expression

$$P(\boldsymbol{\rho}) = \frac{\rho^2}{\boldsymbol{\rho}^2 + 2S_0^2\left[(k/B)^2\,\delta_0^2 S_0^2 - 1\right]}. \tag{45}$$

We calculate in Fig. 7 the degree of polarization of the focused SCRP beam versus the transverse coordinate ρ_x ($\rho_y = 0$) for different values of the initial coherence width δ_0

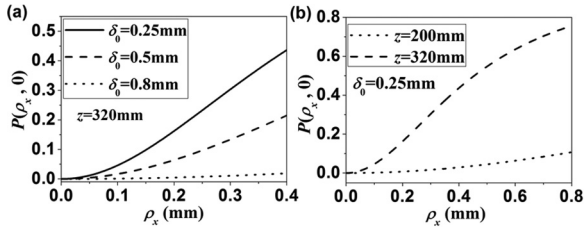

FIG. 7. The degree of polarization of the focused SCRP beam versus the transverse coordinate ρ_x ($\rho_y = 0$) for different values of the initial coherence width δ_0 and the propagation distance.

and the propagation distance with $f = 400$ mm, $\lambda = 632.8$nm, and $\sigma_0 = 1$ mm. One finds from Fig. 7 that the degree of polarization of the focused SCRP beam increases as the transverse coordinate increases or the propagation distance increases or the initial coherence width decreases due to fact that the contribution of the completely polarized part increases as expected. The degree of polarization along the axis of the beam $\rho_x = \rho_y = 0$ always equals to zero, and this can be explained by the fact that the on-axis intensity of the completely polarized part always vanishes.

IV. EXPERIMENTAL GENERATION OF A SCRP BEAM

In this section, we report about the experimental generation of a typical SCRP for the first time and carry out experimental study of its focusing properties.

Figure 8 shows our experimental setup for generating a SCRP beam and measuring the degree of coherence, correlation functions and the focused intensity. A linearly polarized He-Ne laser beam with $\lambda = 632.8$nmpasses through a radial polarization converter (RPC) and becomes a RP beam whose vectorial electric field is expressed as [3]

$$\mathbf{E}(\mathbf{v}) = E_x(\mathbf{v})\mathbf{e}_x + E_y(\mathbf{v})\mathbf{e}_y = \left[\frac{v_x}{\omega_0}\exp\left(-\frac{\mathbf{v}^2}{\omega_0^2}\right)\mathbf{e}_x + \frac{v_y}{\omega_0}\exp\left(-\frac{\mathbf{v}^2}{\omega_0^2}\right)\mathbf{e}_y\right], \quad (46)$$

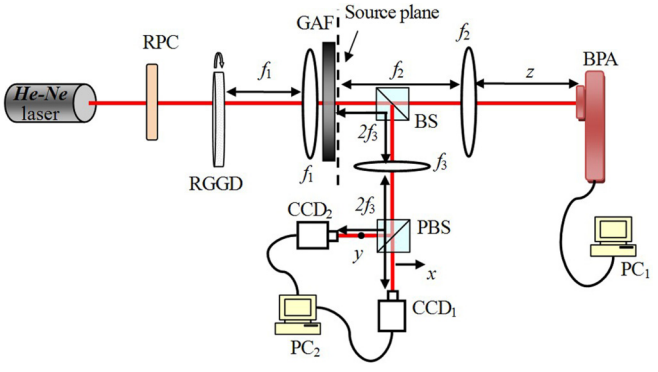

FIG. 8. (Color online) Experimental setup for generating a SCRP beam and measurement of the degree of coherence, correlation functions, and the focused intensity. RPC, radial polarization converter; RGGD, rotating ground-glass disk; L_1, L_2, L_3, thin lenses; GAF, Gaussian amplitude filter; BS, beam splitter; PBS, polarization beam splitter; BPA, beam profile analyzer; CCD_1, CCD_2, charge-coupled devices; PC_1, PC_2, personal computers.

where $\mathbf{e}_\alpha$ denotes the unit vector along αaxis. The BCP matrix of the radially polarized beam reads as

$$\hat{F}(\mathbf{v}_1,\mathbf{v}_2) = \frac{1}{\omega_0^2}\exp\left(-\frac{\mathbf{v}_1^2+\mathbf{v}_2^2}{\omega_0^2}\right)\begin{pmatrix} v_{1x}v_{2x} & v_{1x}v_{2y} \\ v_{1y}v_{2x} & v_{1y}v_{2y}\end{pmatrix}. \quad (47)$$

The RP beam emitted from the RPC illuminates a rotating ground-glass disk (RGGD) producing an incoherent RP beam. As shown in Ref. [73], the transmitted beam from the RGGD can be regarded as an incoherent beam if the diameter of the beam spot of the incident beam is larger than the inhomogeneity scale of the ground glass, and this condition is satisfied in our experiment. The BCP matrix of the incoherent RP beam is given by Eq. (11). After passing through the thin lens L_1 with focal length f_1 and the Gaussian amplitude filter (GAF), the generated incoherent RP beam becomes a SCRP beam, whose BCP matrix elements are given by Eqs. (13)–(15).

The generated SCRP beam is split into two beams by the beam splitter (BS). The transmitted beam passes through the thin lens L_2 with focal length f_2 and arrives at the beam profile analyzer (BPA), which is connected to a personal computer (PC_1) and is used to measure the intensity distribution of the RP beam. The distance from the GAF (source plane) to L_2 equals to f_2 and the distance from L_2 to the BPA equals to z, thus the transfer matrix between the GAF and the BPA is given by Eq. (27) just by replacing f with f_2.

In order to measure the correlation functions and the degree of coherence of the generated partially coherent RP beam, the reflected beam from the BS passes through the thin lens L_3 with focal length f_3 and then is further split into two distinct imaging optical paths by the polarization beam splitter (PBS), the transmitted beam (i.e., x component of the field) and the reflected beam (i.e., y component of the field) from the PBS arrives at two charge-coupled devices CCD_1, CCD_2, respectively. The output signals from CCD_1, CCD_2 are sent to a personal computer (PC_2) to measure the fourth-order correlation functions (i.e., intensity correlation functions). Both the distances from the GAF to L_3 and from L_3 to CCD_1 and CCD_2 are $2f_3$ (i.e., $2f$-imaging system). Therefore, the fourth-order correlation functions of the beam at the detector planes are the same as those in the source plane. The normalized fourth-order correlation functions are expressed as

$$g^{(2)}_{\alpha\beta}(\mathbf{r}_1,\mathbf{r}_2) = \frac{\langle I_\alpha(\mathbf{r}_1,t)I_\beta(\mathbf{r}_2,t)\rangle}{\langle I_\alpha(\mathbf{r}_1,t)\rangle\langle I_\beta(\mathbf{r}_2,t)\rangle}, (\alpha = x,y;\beta = x,y), \quad (48)$$

where the angular brackets denote ensemble average, $I_x(\mathbf{r}_1,t)$and$I_y(\mathbf{r}_2,t)$ represent the instantaneous intensity distributions captured by CCD_1 and CCD_2, respectively. Applying the Gaussian moment theorem, Eq. (48) can be simplified as

$$g^{(2)}_{\alpha\beta}(\mathbf{r}_1,\mathbf{r}_2) = 1 + \gamma^2_{\alpha\beta}(\mathbf{r}_1,\mathbf{r}_2), (\alpha = x,y;\beta = x,y). \quad (49)$$

Equation (49) gives the relationship between the second-order correlation functions and the normalized fourth-order correlation functions. Thus we can determine the correlation functions γ_{xx}, γ_{yy}, and γ_{xy} of the partially coherent RP beam by measuring the fourth-order correlation functions $g^{(2)}_{xx}$, $g^{(2)}_{yy}$, and

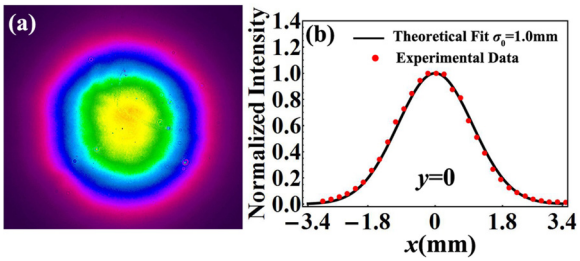

FIG. 9. (Color online) Experimental results of (a) the intensity distribution and (b) the corresponding cross line (dotted curve) of the generated partially coherent RP beam with special correlation functions in the source plane. The solid curve is a result of the theoretical fit.

$g^{(2)}_{xy}$. In a similar way, we can obtain the following relationship between the degree of coherence and the normalized fourth-order correlation function

$$g^{(2)}(\mathbf{r}_1,\mathbf{r}_2) = 1 + \gamma^2(\mathbf{r}_1,\mathbf{r}_2). \tag{50}$$

In our experiment, CCD_1 and CCD_2 capture continuously and synchronously the x component and y component of the intensity distribution of the generated partially coherent RP beam, respectively. Each CCD captures totally 2000 pictures, and each frame is imported into MATLAB to be processed. Each frame captured by CCD_1 or CCD_2 represents one realization of the beam cross section in the detector plane, and each realization is represented as a matrix $I_x^{(n)}(x,y)$ or $I_y^{(n)}(x,y)$, where x and y are pixel spatial coordinates, $I_x^{(n)}$ or $I_y^{(n)}$ is the recorded intensity at that point, n denotes each realization and ranges from 1 to 2000. The correlation functions γ_{xx}, γ_{yy}, and γ_{xy} can be evaluated as

$$\gamma^2_{\alpha\beta}(\mathbf{r}_1,\mathbf{r}_2=0) = \frac{\frac{1}{N}\sum_{n=1}^{N} I_\alpha^{(n)}(x_1,y_1) I_\beta^{(n)}(0,0)}{\bar{I}_\alpha(x_1,y_1)\bar{I}_\beta(0,0)}, \times (\alpha = x,y;\beta = x,y), \tag{51}$$

where $\bar{I}_\alpha(x_1,y_1) = \sum_{n=1}^{N} I_\alpha^{(n)}(x_1,y_1)/N$ denotes the average intensity of all realizations, and $\bar{I}_\beta(0,0) = \sum_{n=1}^{N} I_\beta^{(n)}(0,0)/N$ denotes the average intensity of all realizations at the central point.

In order to measure the degree of coherence of the generated partially coherent RP beam, we remove the PBS in Fig. 8, and then the CCD_1 captures the total intensity distribution and also captures totally 2000 pictures, each frame (i.e., realization) is represented as a matrix $I^{(n)}(x,y)$. The degree of coherence is evaluated as

$$\gamma^2(\mathbf{r}_1,\mathbf{r}_2=0) = \frac{\frac{1}{N}\sum_{n=1}^{N} I^{(n)}(x_1,y_1) I^{(n)}(0,0)}{\bar{I}(x_1,y_1)\bar{I}(0,0)}, \tag{52}$$

with $\bar{I}(x_1,y_1) = \sum_{n=1}^{N} I^{(n)}(x_1,y_1)/N$ and $\bar{I}(0,0) = \sum_{n=1}^{N} I^{(n)}(0,0)/N$.

Figure 9 shows our experimental results of the intensity distribution and the corresponding cross line (dotted curve) of the generated SCRP beam in the source plane. One finds that the intensity distribution of the beam in the source plane has a Gaussian profile, as expected. Via theoretical fit (solid curve) of the experimental results, we obtain that σ_0 is about 1 mm. Figure 10 shows our experimental results of the square of the degree of coherence $\gamma^2(\mathbf{r}_1,\mathbf{r}_2=0)$, the square of the correlation functions $\gamma^2_{xx}(\mathbf{r}_1,\mathbf{r}_2=0)$, $\gamma^2_{yy}(\mathbf{r}_1,\mathbf{r}_2=0)$, $\gamma^2_{xy}(\mathbf{r}_1,\mathbf{r}_2=0)$ and the corresponding cross lines (dotted curves) of the generated SCRP beam. One finds that the distributions of the square of the degree of coherence and the square of the correlation functions all have non-Gaussian profiles as expected by Fig. 2. By the theoretical fit (solid curve) of the experimental results, we obtain that δ_0 is about 0.5 mm. In our experiment, we can adjust the value of δ_0 by varying the value of f_1 in Fig. 8.

Figure 11 shows our experimental results of the intensity distribution and the corresponding cross line (dotted curve) of the generated SCRP beam after its passing through the thin lens L_2 at several propagation distances for the case of $\delta_0 = 0.5$ mm. Figure 12 shows our experimental results of the intensity distribution and corresponding cross line (dotted curve) of the generated SCRP beam in the geometrical focal plane for different values of the initial coherence width δ_0. For the convenience of comparison, the corresponding theoretical

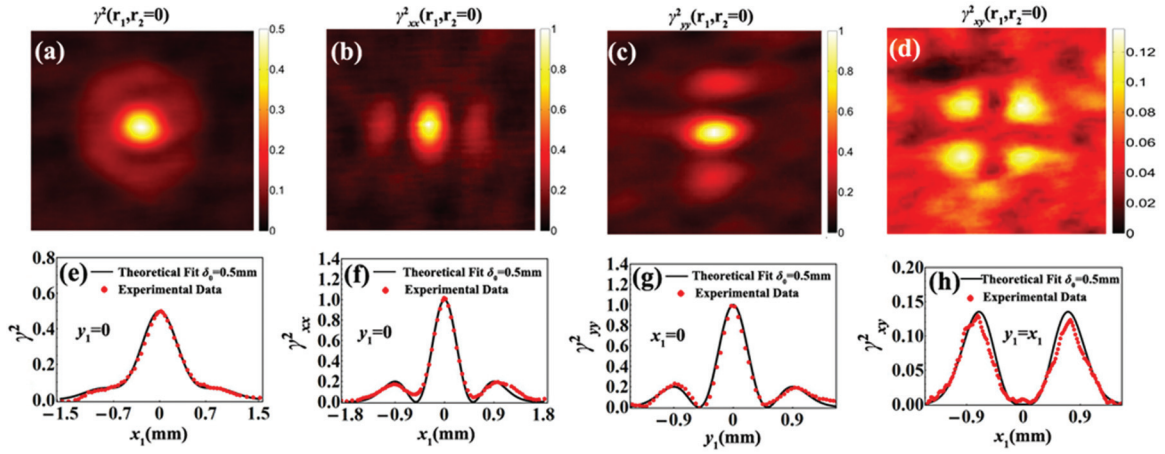

FIG. 10. (Color online) Experimental results of the square of the degree of coherence $\gamma^2(\mathbf{r}_1,\mathbf{r}_2=0)$, the square of the correlation functions $\gamma^2_{xx}(\mathbf{r}_1,\mathbf{r}_2=0)$, $\gamma^2_{yy}(\mathbf{r}_1,\mathbf{r}_2=0)$, $\gamma^2_{xy}(\mathbf{r}_1,\mathbf{r}_2=0)$ and the corresponding cross lines (dotted curves) of the generated SCRP beam. The solid curve is a result of the theoretical fit.

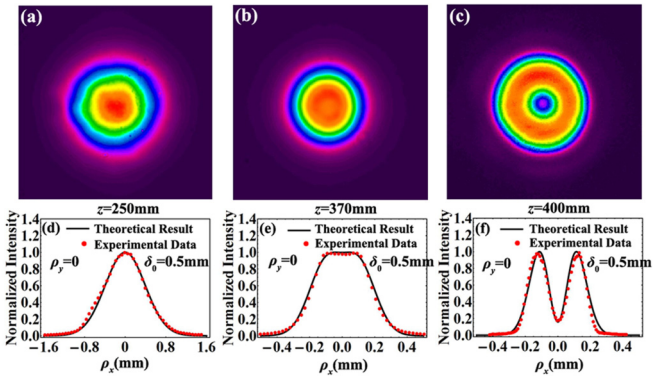

FIG. 11. (Color online) Experimental results of the intensity distribution and corresponding cross line (dotted curve) of the generate beam after passing through the thin lens L_2 at several propagation distances for the case of$\delta_0 = 0.5$ mm. The solid curve is the theoretical result.

results (solid curves) calculated by Eq. (26) are also shown in Figs. 11 and 12. One sees from Fig. 11 that the beam profile of the generated partially coherent RP beam after passing through the thin lens gradually transforms from a Gaussian beam profile to a dark hollow beam on propagation as expected by Fig. 3, and a flat-topped beam profile can be formed at suitable propagation distance. One finds from Fig. 12 that the intensity profile of the generated SCRP beam in the geometrical focal plane gradually transforms from a dark hollow beam profile to a Gaussian beam profile with the increase of δ_0 as expected by Fig. 4, and a flat-topped beam profile can be formed for suitable value of δ_0. Our experimental results agree well with the theoretical predictions.

The degree of polarization of the SCRP beam can be measured through the procedure used in Ref. [34]. Figure 13 shows our experimental results of the degree of polarization of the beam after passing the thin lens versus the transverse coordinate ρ_x $(\rho_y = 0)$ for different values of the initial coherence width δ_0 and the propagation distance. For the convenience of comparison, the corresponding theoretical results calculated by Eq. (45) are also shown in Fig. 13. One

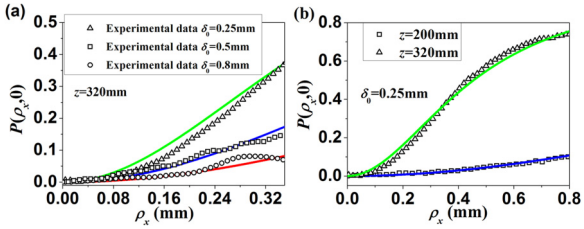

FIG. 13. (Color online) Experimental results of the degree of polarization of the generated SCRP beam after passing the thin lens versus the transverse coordinate ρ_x $(\rho_y = 0)$ for different values of the initial coherence width δ_0 and the propagation distance. The solid curve is the theoretical result.

finds from Fig. 13 that the degree of polarization increases as the transverse coordinate increases or the propagation distance increases or the initial coherence width decreases as expected by Fig. 7. Our experimental results are also consistent with the theoretical results.

V. CONCLUSION

As a summary, we have outlined briefly the sufficient condition for constructing the BCP matrix of a partially coherent vector beam, and we have proposed an optical system for generating a partially coherent vector beam with special correlation functions. In particular, we have introduced the theoretical model for a class of partially coherent RP beam with special correlation functions (SCRP) and derived its propagation formula. Furthermore, we have carried out the experimental generation of the SCRP beam, studied its focusing properties both experimentally and theoretically, and verified that our experimental results agree well the theoretical predictions. Our results have shown that a SCRP beam displays unique features on propagation properties, which are substantially different from those of a RP beam with conventional Schell-model correlation functions. Our results will be useful in particle trapping and material thermal processing.

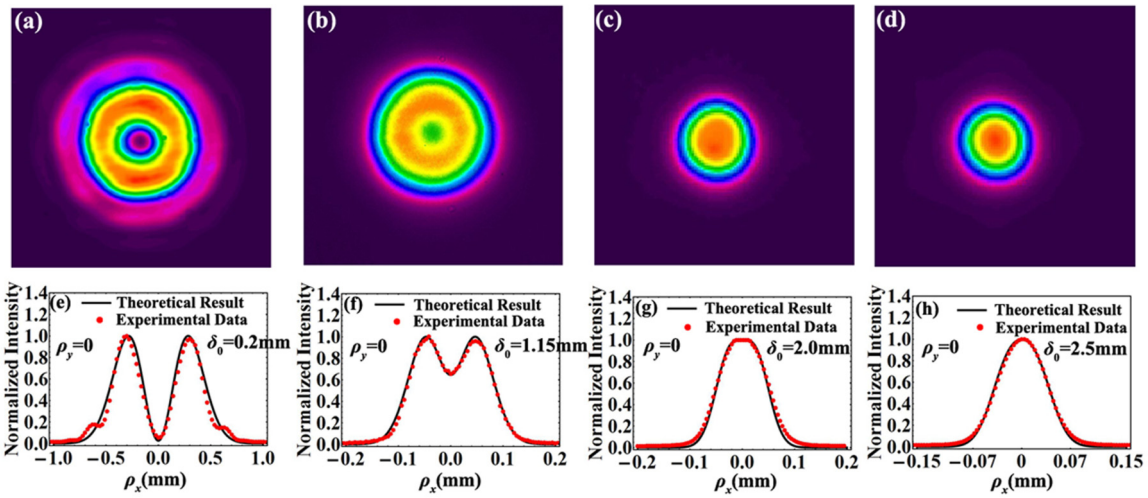

FIG. 12. (Color online) Experimental results of the intensity distribution and corresponding cross line (dotted curve) of the generated SCRP beam in the geometrical focal plane for different values of the initial coherence width δ_0. The solid curve is the theoretical result.

ACKNOWLEDGMENTS

This work is supported by the National Natural Science Foundation of China under Grants No. 11274005, No. 11104195, and No. 11374222, the Huo Ying Dong Education Foundation of China under Grant No. 121009, the Key Project of Chinese Ministry of Education under Grant No. 210081, the Universities Natural Science Research Project of Jiangsu Province under Grants No. 11KJB140007 and No. 10KJB140011, the Project Funded by the Priority Academic Program Development of Jiangsu Higher Education Institutions, and the Project Sponsored by the Scientific Research Foundation for the Returned Overseas Chinese Scholars, State Education Ministry. O.K.'s research is sponsored by US AFOSR (Grant No. FA9550-12-1-0449) and US ONR (Grant No. N00189-12-T-0136).

[1] L. Mandel and E. Wolf, *Optical Coherence and Quantum Optics* (Cambridge University Press, Cambridge, 1995).
[2] C. Brosseau, *Fundamentals of Polarized Light: A Statistical Approach* (Wiley, New York, 1998).
[3] Q. Zhan, Adv. Opt. Photon. **1**, 1 (2009).
[4] D. James, J. Opt. Soc. Am. A **11**, 1641 (1994).
[5] F. Gori, Opt. Lett. **23**, 241 (1998).
[6] E. Wolf, Phys. Lett. A **312**, 263 (2003).
[7] E. Wolf, Opt. Lett. **28**, 1078 (2003).
[8] E. Wolf, *Introduction to the Theory of Coherence and Polarization of Light* (Cambridge University Press, Cambridge, 2007).
[9] O. Korotkova, M. Salem, and E. Wolf, Opt. Lett. **29**, 1173 (2004).
[10] O. Korotkova and E. Wolf, Opt. Commun. **246**, 35 (2005).
[11] O. Korotkova and E. Wolf, Opt. Lett. **30**, 198 (2005).
[12] J. Tervo, T. Setälä, and A. T. Friberg, Opt. Express **11**, 1137 (2003).
[13] K. Lindfors, A. Priimagi, T. Setälä, A. Shevchenko, and A. T. Friberg, Nature Photon. **1**, 228 (2007).
[14] O. Korotkova and E. Wolf, Phys. Rev. E **75**, 056609 (2007).
[15] F. Gori, M. Santarsiero, R. Borghi, and V. Ramírez-Sánchez, J. Opt. Soc. Am. A **25**, 1016 (2008).
[16] O. Korotkova, Opt. Commun. **281**, 2342 (2008).
[17] M. Salem and E. Wolf, Opt. Lett. **33**, 1180 (2008).
[18] M. Yao, Y. Cai, H. T. Eyyuboğlu, Y. Baykal, and O. Korotkova, Opt. Lett. **33**, 2266 (2008).
[19] Y. Cai, O. Korotkova, H. T. Eyyuboğlu, and Y. Baykal, Opt. Express **16**, 15834 (2008).
[20] S. Sahin and O. Korotkova, Phys. Rev. A **78**, 063815 (2008).
[21] T. Setälä, K. Lindfors, and A. T. Friberg, Opt. Lett. **34**, 3394 (2009).
[22] C. Zhao, Y. Cai, and O. Korotkova, Opt. Express **17**, 21472 (2009).
[23] S. Sahin, Z. Tong, and O. Korotkova, Opt. Commun. **283**, 4512 (2010).
[24] S. Zhu, Y. Cai, and O. Korotkova, Opt. Express **18**, 12587 (2010).
[25] Z. Tong, Y. Cai, and O. Korotkova, Opt. Commun. **283**, 3838 (2010).
[26] I. Vidal, E. J. S. Fonseca, and J. M. Hickmann, Phys. Rev. A **84**, 033836 (2011).
[27] F. Wang, G. Wu, X. Liu, S. Zhu, and Y. Cai, Opt. Lett. **36**, 2722 (2011).
[28] G. Wu and Y. Cai, Opt. Express **19**, 8700 (2011).
[29] A. S. Ostrovsky, M. A. Olvera-Santamaria, and P. C. Romero-Soria, Opt. Lett. **36**, 1677 (2011).
[30] Y. Dong, Y. Cai, C. Zhao, and M. Yao, Opt. Express **19**, 5979 (2011).
[31] Y. Dong, F. Feng, Y. Chen, C. Zhao, and Y. Cai, Opt. Express **20**, 15908 (2012).
[32] Y. Dong, F. Wang, C. Zhao, and Y. Cai, Phys. Rev. A **86**, 013840 (2012).
[33] F. Wang, Y. Cai, Y. Dong, and O. Korotkova, Appl. Phys. Lett. **100**, 051108 (2012).
[34] G. Wu, F. Wang, and Y. Cai, Opt. Express **20**, 28301 (2012).
[35] F. Wang, X. Liu, L. Liu, Y. Yuan, and Y. Cai, Appl. Phys. Lett. **103**, 091102 (2013).
[36] S. Zhu, X. Zhu, L. Liu, F. Wang, and Y. Cai, Opt. Express **21**, 27682 (2013).
[37] R. Dorn, S. Quabis, and G. Leuchs, Phys. Rev. Lett. **91**, 233901 (2003).
[38] B. Sick, B. Hecht, and L. Novotny, Phys. Rev. Lett. **85**, 4482 (2000).
[39] K. S. Youngworth and T. G. Brown, Opt. Express **7**, 77 (2000).
[40] L. Novotny, M. R. Beversluis, K. S. Youngworth, and T. G. Brown, Phys. Rev. Lett. **86**, 5251 (2001).
[41] P. Wróbel, J. Pniewski, T. J. Antosiewicz, and T. Szoplik, Phys. Rev. Lett. **102**, 183902 (2009).
[42] H. Wang, L. Shi, B. Lukyanchuk, C. J. R. Sheppard, and C. T. Chong, Nature Photon. **2**, 501 (2008).
[43] W. Chen, D. Abeysinghe, R. Nelson, and Q. Zhan, Nano Lett. **9**, 4320 (2009).
[44] C. Hnatovsky, V. Shvedov, W. Krolikowski, and A. Rode, Phys. Rev. Lett. **106**, 123901 (2011).
[45] H. Ono, H. Wakabayashi, T. Sasaki, A. Emoto, T. Shioda, and N. Kawatsuki, Appl. Phys. Lett. **94**, 071114 (2009).
[46] J.-X. Li, Y. I. Salamin, B. J. Galow, and C. H. Keitel, Phys. Rev. A **85**, 063832 (2012).
[47] S. Payeur, S. Fourmaux, B. E. Schmidt, J. P. MacLean, C. Tchervenkov, F. Legare, M. Piche, and J. C. Kieffer, Appl. Phys. Lett. **101**, 041105 (2012).
[48] R. Oron, S. Blit, N. Davidson, A. A. Friesem, Z. Bomzon, and E. Hasman, Appl. Phys. Lett. **77**, 3322 (2000).
[49] H. Kang, B. Jia, J. Li, D. Morrish, and M. Gu, Appl. Phys. Lett. **96**, 063702 (2010).
[50] H. Lajunen and T. Saastamoinen, Opt. Lett. **36**, 4104 (2011).
[51] L. Waller, G. Situ, and J. W. Fleisher, Nature Photon. **6**, 474 (2012).
[52] Z. Tong and O. Korotkova, Opt. Lett. **37**, 3240 (2012).
[53] S. Sahin and O. Korotkova, Opt. Lett. **37**, 2970 (2012).
[54] O. Korotkova, S. Sahin, and E. Shchepakina, J. Opt. Soc. Am. A **29**, 2159 (2012).
[55] Z. Mei and O. Korotkova, Opt. Lett. **38**, 91 (2013).
[56] H. Lajunen and T. Saastamoinen, Opt. Express **21**, 190 (2013).
[57] F. Wang, X. Liu, Y. Yuan, and Y. Cai, Opt. Lett. **38**, 1814 (2013).
[58] Z. Mei and O. Korotkova, Opt. Lett. **38**, 2578 (2013).

[59] S. Du, Y. Yuan, C. Liang, and Y. Cai, Opt. Laser Technol. **50**, 14 (2013).
[60] Y. Yuan, X. Liu, F. Wang, Y. Chen, Y. Cai, J. Qu, and H. T. Eyyuboğlu, Opt. Commun. **305**, 57 (2013).
[61] Z. Tong and O. Korotkova, J. Opt. Soc. Am. A **29**, 2154 (2012).
[62] Z. Mei, O. Korotkova, and E. Shchepakina, J. Opt. **15**, 025705 (2013).
[63] Z. Mei and O. Korotkova, Opt. Express **21**, 27246 (2013).
[64] F. Gori and M. Santarsiero, Opt. Lett. **32**, 3531 (2007).
[65] F. Gori, V. Ramirez-Sanchez, M. Santarsiero, and T. Shirai, J. Opt. A: Pure Appl. Opt. **11**, 085706 (2009).
[66] F. Gori, M. Santarsiero, S. Vicalvi, R. Borghi, and G. Guattari, J. Eur. Opt. Soc. A Pure Appl. Opt. **7**, 941 (1998).
[67] S. A. Collins, J. Opt. Soc. Am. **60**, 1168 (1970).
[68] Q. Lin and Y. Cai, Opt. Lett. **27**, 216 (2002).
[69] Y. Zhang, B. Ding, and T. Suyama, Phys. Rev. A **81**, 023831 (2010).
[70] C. Zhao and Y. Cai, Opt. Lett. **36**, 2251 (2011).
[71] D. W. Coutts, IEEE J. Quantum Electron. **38**, 1217 (2002).
[72] N. Nishi, T. Jitsuno, K. Tsubakimoto, S. Matsuoka, N. Miyanaga, and M. Nakatsuka, Opt. Rev. **7**, 216 (2000).
[73] P. De Santis, F. Gori, G. Guattari, and C. Palma, Opt. Commun. **29**, 256 (1979).